Inorganic Chemistry

Article

pubs.acs.org/IC

Subtle Modulation of $Cu_4X_4L_2$ Phosphine Cluster Cores Leads to Changes in Luminescence

Kelly Chen, Jason Shearer, and Vincent J. Catalano*

Department of Chemistry, University of Nevada, 1664 North Virginia Street, Reno, Nevada 89557, United States

Supporting Information

ABSTRACT: A series of $Cu_4X_4(PPh_2py)_2$ compounds (X = Cl (**1**), Br (**2**), I (**3**), PPh_2py = 2-(diphenylphosphino)pyridine) were prepared and characterized using X-ray crystallography, NMR, UV−vis, and luminescence spectroscopy. The copper chloride and bromide clusters have Cu_4X_4 octahedral cores while the copper iodide clusters contain an unprecedented butterfly shaped core. Crystallization of the copper bromide and iodide clusters from the appropriate solvent produced the solvates **2**·$2CH_2Cl_2$, **2**·$2CHCl_3$, and **3**·$0.5CH_2Cl_2$ where the presence of the lattice solvate influences the overall structural properties. Using TD-DFT calculations, the emission was assigned to a mixed metal- and halide-to-ligand charge transfer, (M + X)LCT. Subtle differences in the copper core geometry and μ-halide bonding perturb the emissions of these copper(I) halide clusters.

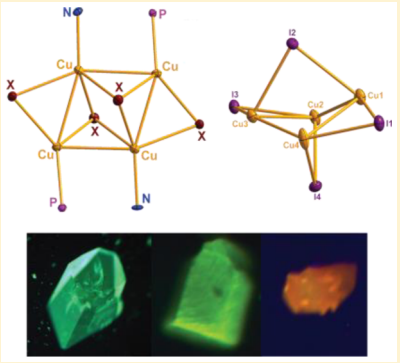

INTRODUCTION

Copper halide clusters have been extensively studied due to their unusual structural and photophysical properties.[1−7] These clusters exhibit a remarkable number of structural motifs including cubane,[1,2,8−14] staircase,[15−17] butterfly,[18,19] extended networks,[20] etc. Multidentate phosphines are often employed to stabilize cuprous halide clusters,[7,18,21−29] and recently, Baumann, Bräse, and co-workers reported a series of intensely luminescent dinuclear $Cu_2I_2L_3$ butterfly clusters with bridging phosphinopyridyl ligands with the emission assigned to a mixed halide- and metal-to-ligand charge transfer, (M + X)LCT, process. Substitution of the pyridyl group dramatically varies the LUMO enabling the emission to span the entire visible spectrum.[21,30−32] These optical properties make Cu(I) phosphine complexes attractive targets for OLED applications.[4,6,21,33−36]

Copper cubanes are the most widely studied structural motif. These complexes often exhibit temperature-dependent dual emission bands which have been assigned to triplet halide-to-ligand charge transfer (^{3}XLCT) and cluster-centered (^{3}CC) transitions.[1,8,9,20,22,37] Vega and Saillard surveyed known copper cubane clusters and determined that the ^{3}CC bands are composed of mainly a $Cu_4(3d) \rightarrow Cu_4(s/p)$ transition.[38] Perruchas and co-workers also reported a series of copper cubanes with various phosphines and computationally assigned the dual emission to a high energy, mixed charge transfer (M +X)LCT and low energy ^{3}CC transition.[22] The ^{3}CC transition occurs through distortions of the Cu_4X_4 core in the excited state, an effect enhanced by strong cuprophilic interactions.[39] As noted by Kitagawa et al., the flexibility in the Cu_4X_4 core is the key factor that influences the photoemissive properties of these complexes.[9]

Octahedral $Cu_4X_4L_2$ motifs also possess interesting photophysical properties but are less-studied relative to the cubane $Cu_4X_4L_4$ compounds. In the octahedral motif, a tetranuclear copper core defines the basal plane of an octahedron with two capping ligands in the apical positions and bridging halides along the meridian. Most clusters with this motif feature P^P ligands supporting the tetranuclear copper core;[23,26,28,29,40−43] however, more recently, complexes with P^N ligands have been reported.[44] Thompson and co-workers reported a series of octahedral copper iodide compounds, $Cu_4I_4(R_2PCH_2py)_2$, that exhibit distinct temperature-dependent high (400−500 nm) and low energy emission bands (500−700 nm) similar to those found in copper cubanes. However, increasing the steric bulk of the phosphine ligands produces complexes with only one high energy band. Thompson and co-workers reasoned that the absence of a ^{3}CC band was due to the inability of the copper core to distort its geometry due to the presence of the bulky ligands.[44]

Recently, we reported a series of $[AuCu(PPh_2py)_3]^{2+}$ pseudopolymorphs where subtle, noncovalent interactions produced drastically different emission properties.[45] We questioned whether similar alterations in optical properties would exist in the homometallic Cu(I) complexes. Here we report the structural and optical properties of a series of $Cu_4X_4(PPh_2py)_2$ complexes where subtle variations in crystallization solvent produce marked structural and optical changes.

RESULTS

As shown in Scheme 1, copper halide clusters $Cu_4X_4(PPh_2py)_2$, where X = Cl (**1**), Br (**2**), I (**3**), were prepared in poor to good

Received: February 27, 2015
Published: June 12, 2015

DOI: 10.1021/acs.inorgchem.5b00443
Inorg. Chem. 2015, 54, 6245−6256

Scheme 1. Preparation of $Cu_4X_4(PPh_2py)_2$ Clusters

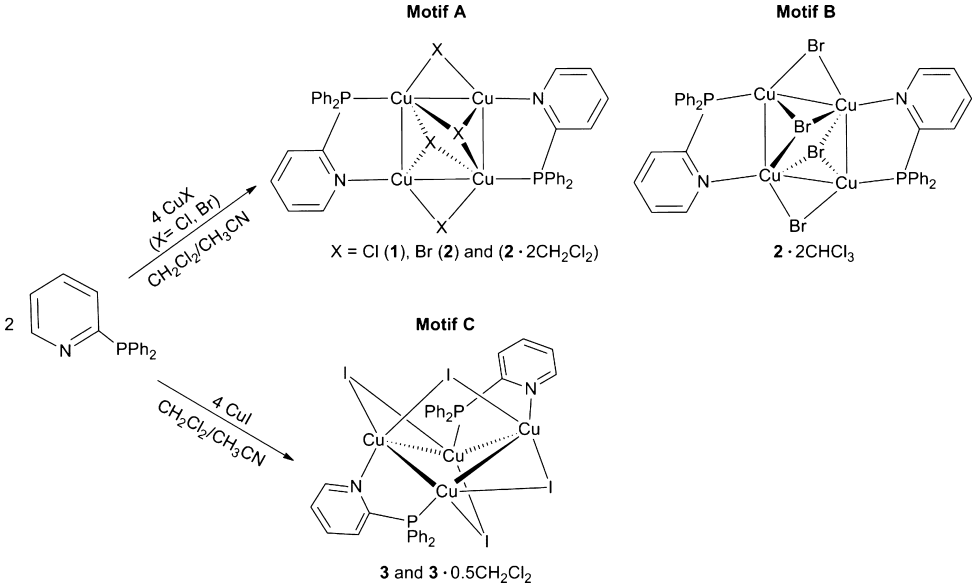

yields by simply mixing the appropriate copper halide with 2-(diphenylphosphino)pyridine in a dichloromethane/acetonitrile solution. The precipitated clusters contain a tetranuclear copper core with two head-to-tail bridging phosphinopyridyl ligands and four bridging halides. Two halide ions doubly bridge neighboring copper atoms of the cluster while the remaining halides either doubly (compound **3**) or triply (compounds **1** and **2**) bridge the metal centers on opposing Cu_4 cluster faces. The compounds are insoluble in most organic solvents but are moderately soluble in dichloromethane and acetonitrile. Compounds **1**−**3** were characterized by ^{1}H NMR spectroscopy; however, the limited solubility of **2** and **3** prevented their characterization by $^{31}P\{^1H\}$ NMR spectroscopy. In acetonitrile, the copper clusters are dynamic as suggested by the broad peaks in the ^{1}H NMR spectra and the $^{31}P\{^1H\}$ NMR spectrum of **1**. NMR spectra are presented in Figures S1−S5 in the Supporting Information (SI).

Remarkably, the solid-state structures of the copper clusters are heavily influenced by choice of crystallization solvent. X-ray quality crystals were obtained by vapor diffusion of diethyl ether into solutions of **1**−**3** to give crystal structures of green/yellow-luminescent **1**, green-luminescent **2**, green-luminescent **2**·2CHCl$_3$, green/yellow-luminescent **2**·2CH$_2$Cl$_2$, green-luminescent **3**, and orange-luminescent **3**·0.5CH$_2$Cl$_2$. Exposing crystals of the solvated complexes **2**·2CHCl$_3$, **2**·2CH$_2$Cl$_2$, and **3**·0.5CH$_2$Cl$_2$ to air or heat did not produce the solvent-free copper clusters. X-ray crystallographic data of the compounds are listed in Table 1. As shown in Scheme 1, the $Cu_4X_4(PPh_2py)_2$ clusters crystallize in three distinct structural motifs: **A**, **B**, and **C** based upon halide binding and core geometry. The core structures of each cluster are shown in Figure 1 while selected bond distances and angles are listed in Tables 2−6. Complete thermal ellipsoid plots and crystallographic data are presented in Figures S6−S14 and Tables S1−S24 in the Supporting Information, respectively.

The structures adopting motif **A** (**1**, **2**, and **2**·2CH$_2$Cl$_2$) contain a planar copper core with two μ_3-halide ions each bridging two P-bound copper atoms and one N-bound copper. In motif **B** (**2**·2CHCl$_3$), the copper core forms a parallelogram with two μ_3-bromide ions each bridging the two N-bound copper atoms and one P-bound copper. In motif **C** (**3** and **3**·0.5CH$_2$Cl$_2$), the copper iodide cluster adopts a butterfly core with four bridging μ_2-iodide ions. Similar to the clusters in motifs **A** and **B**, two halide ions bridge adjacent copper atoms in motif **C**. However, two additional μ_2-iodide ions also bridge opposing copper atoms. At the apex, one iodide ion bridges the two N-bound copper atoms while the other iodide ion bridges the two P-bound copper atoms below the cluster.

The clusters in motif A (**1**, **2**, **2**·2CH$_2$Cl$_2$) are very similar as shown by their structural overlays (Figures S15 and S16 in Supporting Information). The copper chloride cluster **1** crystallizes in the $P2_1/n$ space group with one-half of the complex in the asymmetric unit and the other half generated by inversion. In this green/yellow-luminescent **1**, the Cu−Cu distances are similar (Cu1−Cu2 =2.7254(8) Å and Cu1−Cu2A = 2.7104(8) Å). The copper core is close to rectangular with a Cu2−Cu1−Cu2A angle of 93.89(3)° and a Cu1−Cu2−Cu1A angle of 86.11(3)°. The μ_2-chloride ions doubly bond to adjacent copper atoms with a Cu1−Cl1 distance of 2.2869(11) Å and Cu2A−Cl1 distance of 2.4069(12) Å, and these chloride ions are positioned 0.6711(14) Å above and below the rigorously planar copper core. The other chloride ions triply bond to the copper core; however, the bonding is dissymmetric. The chloride is closest to one N-bound copper with a Cu2A−Cl2 distance of 2.2701(11) Å and intermediate to one of the P-bound copper atoms with a Cu1−Cl2 distance of 2.4135(11) Å. There is a longer interaction between Cl2 and the other P-bound copper atom with a Cu1A−Cl2 distance of 2.6990(11) Å. Additionally, there is a long nonbonding interaction between the chloride and the remaining N-bound copper (Cu2···Cl2 = 2.9932(11) Å). As shown in Figure S7 in the Supporting Information, there is a long intermolecular $\pi_{ph}-\pi_{ph}$ interaction of 3.8050(3) Å between the centroids of the phenyl rings of the copper cluster.

The green-luminescent copper bromide cluster **2** also crystallizes in the $P2_1/n$ space group. Similar to **1**, one-half of **2** appears in the asymmetric unit, and the entire complex is generated by inversion. The Cu−Cu separations differ with Cu1−Cu2 measuring 2.6411(8) Å which is shorter than the Cu1−Cu2A distance at 2.7168(8) Å. The tetranuclear core of **2**

DOI: 10.1021/acs.inorgchem.5b00443
Inorg. Chem. 2015, 54, 6245−6256

Table 1. X-ray Crystallographic Data for All Copper Halide Species

	1	1a	2	2·2CH_2Cl_2	2·2$CHCl_3$	3	3·0.5CH_2Cl_2
formula	$C_{17}H_{14}Cl_2Cu_2NP$	$C_{19}H_{12}C_{12}Cu_2N_2O_{0.5}P$	$C_{34}H_{28}Br_4Cu_4N_2P_2$	$C_{36}H_{32}Br_4Cl_4Cu_4N_2P_2$	$C_{36}H_{30}Br_4Cl_6Cu_4N_2P_2$	$C_{34}H_{28}Cu_4I_4N_2P_2$	$C_{34.5}H_{29}ClCu_4I_4N_2P_2$
fw	461.24	505.26	1100.32	1270.17	1339.06	1288.28	1330.75
cryst size, mm^3	0.178 × 0.162 × 0.136	0.146 × 0.141 × 0.129	0.256 × 0.166 × 0.106	0.198 × 0.034 × 0.028	0.203 × 0.063 × 0.062	0.16 × 0.082 × 0.072	0.025 × 0.02 × 0.02
cryst syst	monoclinic	triclinic	monoclinic	triclinic	triclinic	monoclinic	monoclinic
space group	$P2_1/n$	$P\bar{1}$	$P2_1/n$	$P\bar{1}$	$P\bar{1}$	$P2_1/c$	$C2/c$
a, Å	12.1022(10)	9.3487(7)	11.8720(6)	10.2258(17)	9.9640(8)	16.6090(7)	36.414(3)
b, Å	11.2109(9)	10.0979(7)	11.6662(6)	11.0279(19)	14.5901(12)	13.7822(6)	14.0071(12)
c, Å	13.1539(11)	11.1299(8)	13.3924(7)	19.447(3)	15.9328(13)	16.3524(7)	16.0994(13)
α, deg	90	103.5980(10)	90	91.880(3)	79.2801(14)	90	90
β, deg	92.0100(10)	93.2370(10)	90.3793(9)	98.999(2)	85.9414(14)	99.8182(8)	108.9400(10)
γ, deg	90	95.7600(10)	90	103.505(3)	72.0265(13)	90	90
V, $Å^3$	1783.6(3)	1012.59(13)	1854.98(17)	2100.7(6)	2164.5(3)	3688.4(3)	7766.9(11)
Z	4	2	2	2	2	4	8
ρ, Mg m^{-3}	1.718	1.657	1.970	2.008	2.055	2.320	2.276
μ, mm^{-1}	2.770	2.451	6.683	6.162	6.106	5.738	5.520
R1 [$I > 2\sigma(I)$]	0.0442	0.0292	0.0329	0.0381	0.0401	0.0345	0.0520
wR2 (all data)	0.1150	0.0753	0.0799	0.0977	0.1001	0.0975	0.1680

is skewed toward a parallelogram with an obtuse Cu2−Cu1−Cu2A angle of 101.46(3)° and an acute Cu1−Cu2−Cu1A angle of 78.54(3)°. The bromide ions doubly bond to adjacent copper atoms with a Cu1−Br1 distance of 2.4362(7) Å and Cu2−Br1 distance of 2.4896(8) Å, and these bromide ions reside 0.6064(11) Å above and below the rigorously planar copper core. In **2**, the triply bound bromide atom is closest to one N-bound copper atom (Cu2−Br2 = 2.3983(7) Å) and approximately equidistant to the P-bound copper atoms (Cu1−Br2 = 2.5805(8) Å and Cu1A−Br2 = 2.5961(8) Å). There is a long nonbonding interaction between the bromide and the remaining N-bound copper (Cu2···Br2 = 3.2400(8) Å). Similarly to **1**, there is a long intermolecular $\pi_{ph}-\pi_{ph}$ interaction of 3.6888(2) Å between the centroids of the phenyl rings of the copper cluster (Figure S8 in Supporting Information).

Co-crystallization with dichloromethane subtly alters the structure of **2**. Green/yellow-luminescent copper bromide cluster **2**·2CH_2Cl_2 crystallizes in the $P\bar{1}$ space group. As a comparison, the thermal ellipsoid plots of **2** and **2**·2CH_2Cl_2 are shown in Figure 2. In compound **2**·2CH_2Cl_2, the Cu−Cu separations range from 2.6453(11) to 2.7691(9) Å. The copper core adopts a skewed rectangular geometry with obtuse Cu2−Cu1−Cu4 and Cu2−Cu3−Cu4 angles of 92.49(3)° and 93.40(3)° and acute Cu1−Cu2−Cu3 and Cu3−Cu4−Cu1 angles of 85.74(3)° and 87.94(3)°, respectively. The μ_2-bromide ions bond unsymmetrically to the adjacent copper atoms. One bromide is approximately equidistant to two adjacent copper atoms (Cu1−Br1 = 2.4301(8) Å and Cu4−Br1 = 2.4962(9) Å) and resides 0.7061(13) Å below the planar copper core. The other μ_2-bromide is closer to one copper atom (Cu3−Br3 = 2.3979(8) Å) than to the other adjacent copper (Cu2−Br3 = 2.5187(8) Å) and resides 0.6888(12) Å above the planar copper core. The triply bridging bromide ions are closest to the N-bound copper atoms (Cu2−Br4 = 2.397(1) Å and Cu4−Br2 = 2.4299(10) Å). These each bind a neighboring P-bound copper at slightly longer separations (Cu1−Br2 = 2.5129(10) Å and Cu3−Br4 = 2.5515(10) Å). The third interaction to the P-bound copper atom is considerably longer (Cu1−Br4 = 2.8626(11) Å and Cu3−Br2 = 2.7596(11) Å). Additionally, there is a long nonbonding interaction between the bromide ions and the remaining N-bound copper atoms (Cu2···Br2 = 3.1232(11) Å and Cu4···Br4 = 2.9657(11) Å). Two dichloromethane molecules are found in the crystal lattice of **2**·2CH_2Cl_2. One dichloromethane molecule resides close to the pyridyl ring on the diphenylphosphino ligand with a chlorine atom straddling the C13−C14 ring juncture at a distance of 3.3579(4) Å. The Cl3S−$Py_{centroid}$ distance is slightly longer at 3.5621(4) Å. The remaining dichloromethane molecule is positioned near C28 (Cl1S−C28 = 3.286(6) Å) of one of the phenyl rings on the other diphenylphosphinopyridine ligands with a longer Cl1S−$Ph_{centroid}$ separation of 3.3848(5) Å.

Crystallization of **2** from chloroform dramatically alters the halide bonding and distorts the metal core. The green-luminescent bromide cluster **2**·2$CHCl_3$ constitutes the second motif and crystallizes in the $P\bar{1}$ space group. The main difference between motifs **A** and **B** is that, in **B**, the bromide ions now triply bridge two N-bound copper atoms and only one P-bound copper atom (Supporting Information Figure S17). The Cu−Cu distances in **2**·2$CHCl_3$ range from 2.6768(10) to 2.7449(9) Å. The copper core has considerably more distorted Cu1−Cu2−Cu3 and Cu3−Cu4−Cu1 angles of 104.20(3)° and 105.56(3)° and Cu2−Cu3−Cu4 and Cu2−

DOI: 10.1021/acs.inorgchem.5b00443
Inorg. Chem. 2015, 54, 6245−6256

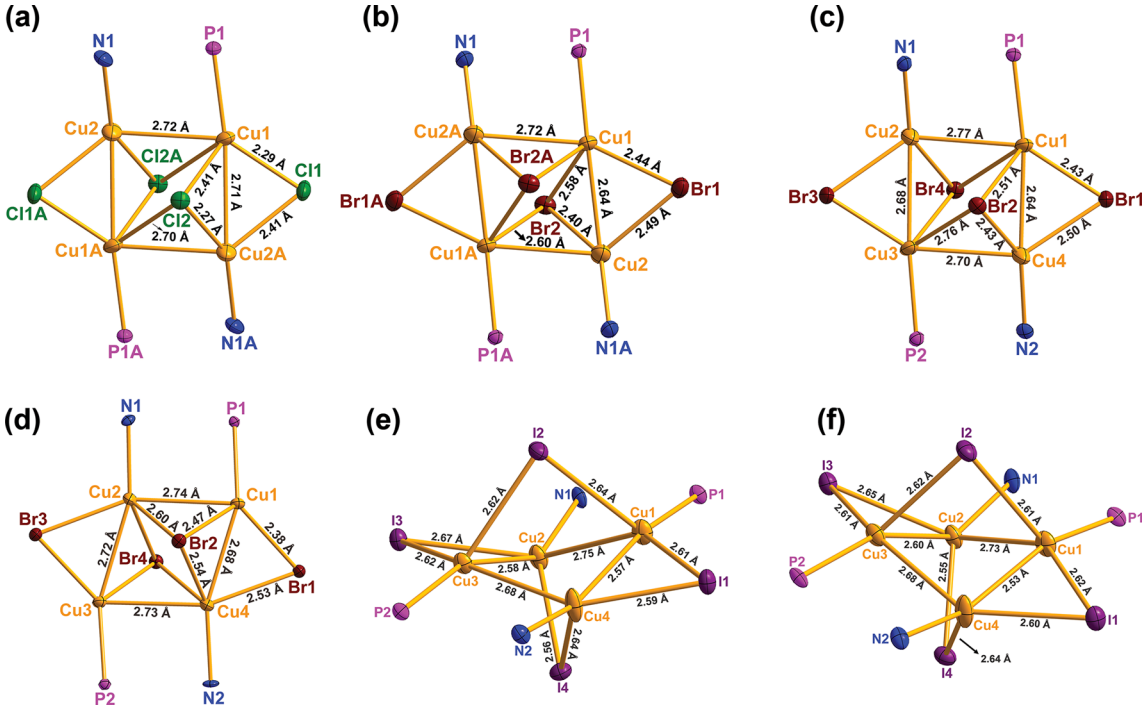

Figure 1. X-ray thermal ellipsoid (50%) plots of the core structures of (a) **1**, (b) **2**, (c) **2**·2CH_2Cl_2, (d) **2**·2$CHCl_3$, (e) **3**, and (f) **3**·0.5CH_2Cl_2.

Table 2. Selected Bond Distances (Å) and Angles (deg) of 1

Cu1−Cu2	2.7254(8)
Cu1−Cu2A	2.7104(8)
Cu1···Cu1A	3.7109(12)
Cu2···Cu2A	3.9720(12)
Cu1−Cl1	2.2869(11)
Cu2A−Cl1	2.4069(12)
Cu1−Cl2	2.4135(11)
Cu2···Cl2	2.9932(11)
Cu1A−Cl2	2.6990(11)
Cu2A−Cl2	2.2701(11)
Cu1−Cl1−Cu2A	70.49(3)
Cu1−Cl2−Cu2A	56.58(2)
Cu1−Cl2−Cu2	65.87(3)
Cu2−Cl2−Cu1A	70.64(3)
Cu1A−Cl2−-Cu2A	59.39(3)
Cu1−Cu2−Cu1A	86.11(3)
Cu2−Cu1−Cu2A	93.89(3)
Cu1−Cu2−Cu1A−Cu2A	0
P1−Cu1−Cu2−N1	−24.91(11)

Table 3. Selected Bond Distances (Å) and Angles (deg) of 2

Cu1−Cu2	2.6411(8)
Cu1−Cu2A	2.7168(8)
Cu1···Cu1A	3.3920(12)
Cu2···Cu2A	4.1481(11)
Cu1−Br1	2.4362(7)
Cu2−Br1	2.4896(8)
Cu1−Br2	2.5805(8)
Cu2−Br2	2.3983(7)
Cu1A−Br2	2.5961(8)
Cu2A···Br2	3.2400(8)
Cu1−Br1−Cu2	64.84(2)
Cu1−Br2−Cu2	63.95(2)
Cu1−Br2−Cu2A	54.224(19)
Cu2−Br2−Cu1A	52.409(18)
Cu1A−Br2−Cu2	65.77(2)
Cu1−Cu2−Cu1A	78.54(3)
Cu2−Cu1A−Cu2A	101.46(3)
Cu1−Cu2−Cu1A−Cu2A	0
P1−Cu1−Cu2−N1	−16.87(11)

Cu1−Cu4 angles of 74.91(3)° and 75.33(3)°. The μ_2-bromide ions are positioned closer to one set of copper atoms (Cu1−Br1 = 2.3830(8) Å and Cu3−Br3 = 2.3920(8) Å) than to the adjacent copper atoms (Cu2−Br3 = 2.5679(8) Å and Cu4−Br1 = 2.5307(9) Å). The μ_2-bromide ions reside above and below the planar copper core (Br1 = 0.7439(14) Å and Br3 = 0.6072(13) Å). The remaining bromide ions triply bridge opposing Cu_4 cluster faces and are closer to the P-bound copper atoms (Cu1−Br2 = 2.4687(9) Å and Cu3−Br4 = 2.4605(9) Å) than to the N-bound copper atoms. The Cu2−Br4 and Cu4−Br2 separations are slightly longer at 2.5012(10) and 2.5389(11) Å, respectively. These bromide ions weakly interact with the remaining N-bound copper centers with Cu2−Br2 and Cu4−Br4 separations of 2.6008(10) and 2.6307(11) Å, respectively. There are additional nonbonding interactions between the bromide ions and the remaining P-bound copper atoms (Cu3···Br2 = 3.3101(10) Å and Cu1···Br4 = 3.2973(10) Å). Like **2**·2CH_2Cl_2, **2**·2$CHCl_3$ also crystallizes with two solvates. One chloroform molecule is positioned near the centroid of the phenyl ring of one of the diphenylphosphinopyridyl ligands with a short Cl6S−π_{Ph} distance of 3.3400(2) Å.

Changing the halide to iodide profoundly alters the cluster core. The copper iodide clusters **3** and **3**·0.5CH_2Cl_2 (motif **C**) adopt a butterfly copper core each with four μ_2-iodide ions as shown in Figure 3. Overlays of **3** and **3**·0.5CH_2Cl_2 (Figure S18 in Supporting Information) show that the two structures are nearly superimposable except for minor twisting of two phenyl rings. In both structures, two iodide ions bridge adjacent copper atoms while two bridge opposing copper atoms. Green-

DOI: 10.1021/acs.inorgchem.5b00443
Inorg. Chem. 2015, 54, 6245−6256

Table 4. Selected Bond Distances (Å) and Angles (deg) of 2·2CH$_2$Cl$_2$

Cu1−Cu2	2.7691(9)	Cu1−Br1−Cu4	64.94(3)
Cu1−Cu4	2.6453(11)	Cu1−Br2−Cu4	64.69(3)
Cu2−Cu3	2.6802(10)	Cu1−Br2−Cu2	57.64(2)
Cu3−Cu4	2.6951(9)	Cu2−Br2−Cu3	53.78(2)
Cu1···Cu3	3.7081(11)	Cu3−Br2−Cu4	62.19(3)
Cu2···Cu4	3.9118(12)	Cu2−Br3−Cu3	66.01(3)
Cu1−Br1	2.4301(8)	Cu1−Br4−Cu4	53.95(2)
Cu4−Br1	2.4962(9)	Cu1−Br4−Cu2	62.80(2)
Cu1−Br2	2.5129(10)	Cu2−Br4−Cu3	65.50(3)
Cu2···Br2	3.1232(11)	Cu3−Br4−Cu4	57.90(2)
Cu3−Br2	2.7596(11)	Cu1−Cu2−Cu3	85.74(3)
Cu4−Br2	2.4299(10)	Cu2−Cu3−Cu4	93.40(3)
Cu2−Br3	2.5187(8)	Cu3−Cu4−Cu1	87.94(3)
Cu3−Br3	2.3979(8)	Cu2−Cu1−Cu4	92.49(3)
Cu1−Br4	2.8626(11)	Cu1−Cu2−Cu3−Cu4	−4.86(3)
Cu2−Br4	2.397(1)	P1−Cu1−Cu2−N1	−27.20(14)
Cu3−Br4	2.5515(10)	P2−Cu3−Cu4−N2	23.72(14)
Cu4···Br4	2.9657(11)		

Table 5. Selected Bond Distances (Å) and Angles (deg) of 2·2CHCl$_3$

Cu1−Cu2	2.7449(9)	Cu1−Br1−Cu4	65.94(3)
Cu1−Cu4	2.6768(10)	Cu1−Br2−Cu4	64.61(3)
Cu2−Cu3	2.7150(9)	Cu1−Br2−Cu2	65.51(3)
Cu3−Cu4	2.7334(10)	Cu2−Br2−Cu3	53.05(2)
Cu1···Cu3	4.3084(10)	Cu3−Br2−Cu4	53.78(3)
Cu2···Cu4	3.3133(10)	Cu2−Br3−Cu3	66.27(2)
Cu1−Br1	2.3830(8)	Cu1−Br4−Cu4	52.22(2)
Cu4−Br1	2.5307(9)	Cu1−Br4−Cu2	54.44(2)
Cu1−Br2	2.4687(9)	Cu2−Br4−Cu3	66.34(3)
Cu2−Br2	2.6008(10)	Cu3−Br4−Cu4	64.84(3)
Cu3···Br2	3.3101(10)	Cu1−Cu2−Cu3	104.20(3)
Cu4−Br2	2.5389(11)	Cu2−Cu3−Cu4	74.91(3)
Cu2−Br3	2.5679(8)	Cu3−Cu4−Cu1	105.56(3)
Cu3−Br3	2.3920(8)	Cu2−Cu1−Cu4	75.33(3)
Cu1···Br4	3.2973(10)	Cu1−Cu2−Cu3−Cu4	0.18(4)
Cu2−Br4	2.5012(10)	P1−Cu1−Cu2−N1	−19.83(17)
Cu3−Br4	2.4605(9)	P2−Cu3−Cu4−N2	17.32(17)
Cu4−Br4	2.6307(11)		

luminescent **3** crystallizes in the $P2_1/c$ space group. Two iodide ions bridge adjacent copper atoms with Cu−I distances ranging from 2.5865(8) to 2.6748(8) Å. These adjacent copper atoms also have similar short Cu−Cu distances (Cu1−Cu4 = 2.5736(12) Å and Cu2−Cu3=2.5827(10) Å). The separations between the other adjacent copper atoms bridged by the same phosphine ligand are longer with Cu1−Cu2 and Cu3−Cu4 measuring 2.7541(10) and 2.6817(11) Å, respectively. The "face-capping" iodide ions doubly bridge opposing copper atoms with Cu−I separations ranging from 2.5577(9) to 2.6388(9) Å. The distances of the nonbonding Cu−I interactions range from 2.8848(9) to 3.3851(9) Å. The dihedral angle between the Cu2−Cu3−Cu4 and Cu2−Cu1−Cu4 planes in the butterfly core is 42.380°. In the extended lattice, an intermolecular π_{Py}−π_{Ph} interaction of 3.6470(1) Å between the centroids of the pyridyl and phenyl rings of the phosphine ligands is observed. The butterfly core does not significantly distort the intermetallic angles relative to the previous two motifs. The Cu2−Cu1−Cu4 and Cu2−Cu3−Cu4 angles measure 90.47(3)° and 91.92(3)° while the Cu1−Cu2−Cu3 and Cu3−Cu4−Cu1 angles measure 80.67(3)° and 82.24(3)°, respectively.

Table 6. Selected Bond Distances (Å) and Angles (deg) of 3 and 3·0.5CH$_2$Cl$_2$

	3	3·0.5CH$_2$Cl$_2$
Cu1−Cu2	2.7541(10)	2.729(3)
Cu1−Cu4	2.5736(12)	2.527(2)
Cu2−Cu3	2.5827(10)	2.596(2)
Cu3−Cu4	2.6817(11)	2.681(3)
Cu1···Cu3	3.4569(11)	3.309(3)
Cu2···Cu4	3.7848(11)	3.821(2)
Cu1−I1	2.6093(9)	2.624(2)
Cu4−I1	2.5865(8)	2.600(3)
Cu1−I2	2.6352(9)	2.607(2)
Cu3−I2	2.6222(9)	2.616(2)
Cu2−I3	2.6748(8)	2.652(2)
Cu3−I3	2.6150(8)	2.609(2)
Cu2−I4	2.5577(9)	2.5479(18)
Cu4−I4	2.6388(9)	2.641(2)
Cu1−I1−Cu4	59.38(3)	57.85(6)
Cu1−I2−Cu3	82.22(3)	78.64(6)
Cu2−I3−Cu3	58.44(2)	59.13(6)
Cu2−I4−Cu3	56.27(2)	56.45(5)
Cu1−Cu2−Cu3	80.67(3)	76.80(8)
Cu2−Cu3−Cu4	91.92(3)	92.77(8)
Cu3−Cu4−Cu1	82.24(3)	78.84(7)
Cu2−Cu1−Cu4	90.47(3)	93.17(9)
Cu1−Cu2−Cu3−Cu4	−27.67(4)	−30.48(6)
P1−Cu1−Cu2−N1	−16.00(15)	−19.5(3)
P2−Cu3−Cu4−N2	−9.07(16)	−8.4(3)

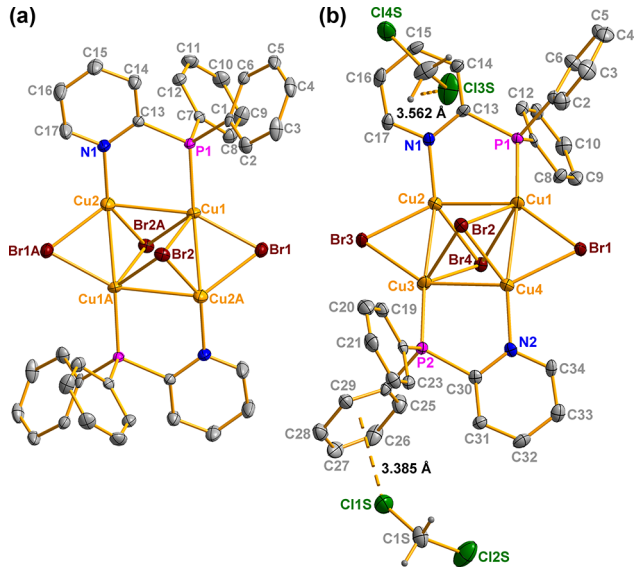

Figure 2. Thermal ellipsoid (50%) plot of (a) **2** and (b) **2**·2CH$_2$Cl$_2$. Hydrogen atoms on copper cluster are excluded for clarity. Hydrogen atoms on solvent molecules are represented as spheres of arbitrary radius.

Crystallization of **3** from dichloromethane does not significantly alter the solid-state structure. Only poorly diffracting crystals of orange-luminescent **3**·0.5CH$_2$Cl$_2$ were obtained. Copper iodide cluster **3**·0.5CH$_2$Cl$_2$ crystallizes in the $C2/c$ space group. As seen in the structure of **3**, two iodide ions bridge adjacent copper atoms, and the remaining two iodide ions bridge opposing copper atoms (Figures S13 and S14 in

DOI: 10.1021/acs.inorgchem.5b00443
Inorg. Chem. 2015, 54, 6245−6256

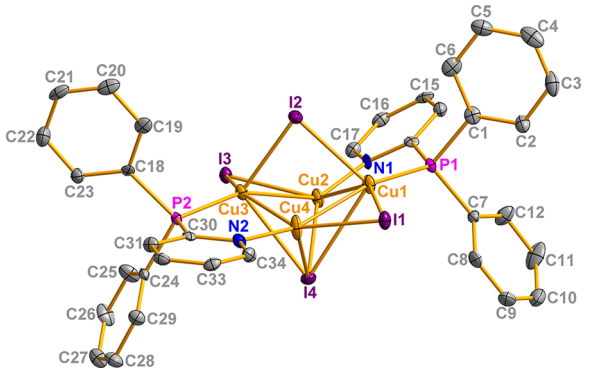

Figure 3. Thermal ellipsoid (50%) plot of **3**. Hydrogen atoms are excluded for clarity.

Supporting Information). Two iodide ions bridge adjacent copper atoms with Cu−I distances ranging from 2.600(3) to 2.652(2) Å. These adjacent copper atoms have similar short Cu−Cu distances (Cu1−Cu4 = 2.527(2) Å and Cu2−Cu3 = 2.596(2) Å). The copper atoms bridged by the same phosphine ligand have longer Cu−Cu distances (Cu1−Cu2 = 2.729(3) Å and Cu3−Cu4 = 2.681(3) Å). The P-bound copper atoms are puckered toward one iodide (Cu1−I2 = 2.607(2) Å and Cu3−I2 = 2.616(2) Å) and have similar intermetallic angles (Cu2−Cu1−Cu4 = 93.17(9)° and Cu2−Cu3−Cu4 = 92.77(8)°). The N-bound copper atoms are closer to the remaining iodide (Cu2−I4 = 2.5479(18) Å and Cu4−I4 = 2.641(2) Å) and have smaller intermetallic angles (Cu1−Cu2−Cu3 = 76.80(8)° and Cu3−Cu4−Cu1 = 78.84(7)°). The dihedral angle between the Cu2−Cu3−Cu4 and Cu2−Cu1−Cu4 planes in the butterfly core is 48.4°. As seen in green-luminescent **3**, there is a similar $\pi_{Py}-\pi_{Ph}$ interaction of 3.6670(2) Å between the centroids of the pyridyl and phenyl rings in orange-luminescent **3**·0.5CH_2Cl_2. Additionally, one dichloromethane molecule in **3**·0.5CH_2Cl_2 resides near the centroid of the pyridyl ring (Cl1S−$Py_{centroid}$ = 3.8671(2) Å) of one of the diphenylphosphinopyridyl ligands and straddles the N2−C34 ring juncture at a distance of 3.5173(2) Å.

When crystals of green-luminescent **1** are grown from acetonitrile/diethyl ether, yellow-luminescent crystals, $Cu_4Cl_4(NCCH_3)_2(PPh_2py)_2$ (**1a**), are obtained as shown in Scheme 2. Compound **1a** crystallizes in the $P\bar{1}$ space group. Selected bond distances and angles are listed in Table 7. The asymmetric unit contains one-half of the molecule with the rest generated by an inversion. While the structure of **1** falls in the motif **A** category, the related **1a** more closely resembles that of motif **B**. As shown in Figure 4, the cluster has a tetranuclear copper core arranged in a parallelogram with two head-to-tail diphenylphosphinopyridyl ligands. Two μ_2-chloride ions bridge the adjacent copper atoms, and two μ_3-chloride ions lie above and below the rigorously planar copper core. Like the copper bromide structure of motif **B**, each μ_3-halide bridges two N-bound copper atoms and one P-bound copper atom. Additionally, each P-bound copper atom is coordinated to one acetonitrile molecule. The Cu−Cu distances in **1a** are long and similar (Cu1−Cu2 = 3.0050(5) Å and Cu1−Cu2A = 2.9963(5) Å). An additional diagonal Cu2−Cu2A interaction of 2.9681(7) Å links the pyridyl-bound copper atoms. The μ_2-chloride ions are skewed toward one set of copper atoms (Cu1−Cl1 = 2.3355(7) Å and Cu2A−Cl1 = 2.4438(7) Å) and reside 0.9264(10) Å above and below the rigorously planar copper core. The μ_3-chloride ions are approximately equidistant

Scheme 2. Crystallization of $Cu_4Cl_4(PPh_2py)_2$

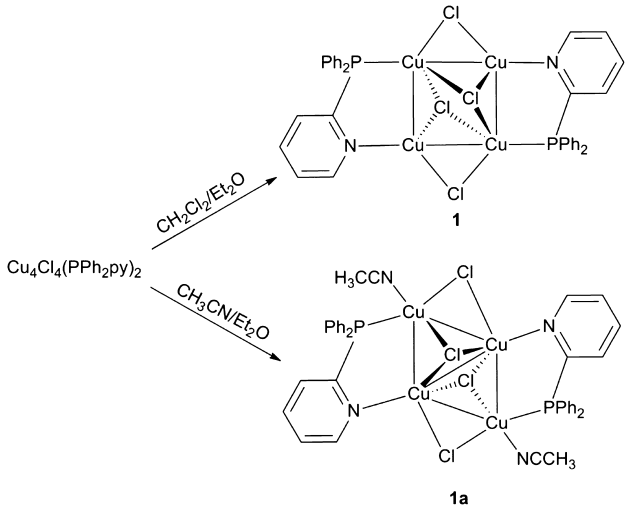

Table 7. Selected Bond Distances (Å) and Angles (deg) of 1a

Cu1−Cu2	3.0050(5)
Cu1−Cu2A	2.9963(5)
Cu1···Cu1A	5.2159(7)
Cu2−Cu2A	2.9681(7)
Cu1−N2	2.086(3)
Cu1−Cl1	2.3355(7)
Cu2A−Cl1	2.4438(7)
Cu1−Cl2	2.4240(7)
Cu2−Cl2	2.3971(7)
Cu1A···Cl2	3.8555(8)
Cu2A-Cl2	2.4076(7)
Cu1−Cl1−Cu2A	77.61(2)
Cu1−Cl2−Cu2A	76.65(2)
Cu1−Cl2−Cu2	77.11(2)
Cu2−Cl2−Cu1A	50.997(16)
Cu1A−Cl2−Cu2A	51.206(15)
Cu1−Cu2−Cu1A	120.716(14)
Cu2−Cu1A−Cu2A	59.284(14)
Cu1−Cu2−Cu1A−Cu2A	0
P1−Cu1−Cu2−N1	28.20(7)

from the three opposing copper atoms (Cu1−Cl2 = 2.4240(7) Å, Cu2−Cl2 = 2.3971(7) Å, and Cu2A−Cl2 = 2.4076(7) Å). The intermetallic angles vary greatly. The angle around the P-bound copper atom is 59.284(14)° for Cu2−Cu1A−Cu2A while the corresponding angle for the N-bound copper atom is 120.716(14)° for Cu1−Cu2−Cu1A.

As seen in Scheme 3, yellow-luminescent crystals of staircase-shaped polymer $(Cu_2Br_2PPh_2py)_n$ (**2a**) were obtained in approximately 10% yield concomitantly with **2**. Compound **2a** also crystallizes in the $P\bar{1}$ space group. The asymmetric unit contains one edge of the Cu_2Br_2 staircase with the remaining coordination polymer generated through an inversion. A common motif in copper halide clusters, the staircase features alternating Cu−Br bonds forming the rungs with long diagonal Cu−Cu bonds (2.9369(12) and 2.9993(17) Å) linking four copper atoms in a row. The diphenylphosphinopyridyl ligands bridge copper atoms along the same side of the staircase. A complete ellipsoid plot and bond table of **2a** are presented in Figure S11 and Tables S16−S18 in the Supporting Information,

DOI: 10.1021/acs.inorgchem.5b00443
Inorg. Chem. 2015, 54, 6245−6256

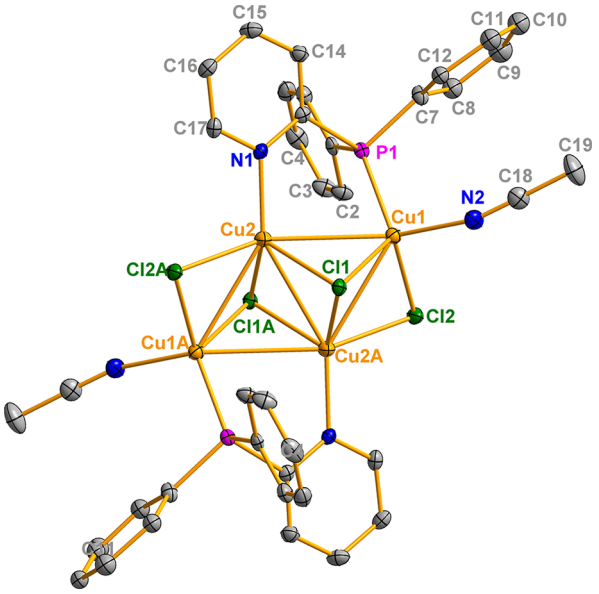

Figure 4. Thermal ellipsoid (50%) plot of **1a**. Hydrogen atoms are excluded for clarity.

respectively. Compounds **1a** and **2a** were obtained as minor products and were only characterized crystallographically.

As noted above, these complexes dissociate upon dissolution presumably into $Cu_2X_2L_2$ dimers, such as those recently reported by Yersin and co-workers.[46] These solutions are photoluminescent with low energy emission bands at 627, 656, and 679 nm for X = Cl, Br, and I, respectively (Figure S19 in Supporting Information). Additional solution and solid-state excitation and emission spectra of **1**−**3** are presented in Figures S20−S25 in the Supporting Information. However, in the solid state, the emission varies as a function of cluster geometry and lattice interactions. For example, as shown in Figure 5, copper chloride **1** is the considerably red-shifted (λ_{max} = 548 nm) compared to the solvent-free copper bromide (λ_{max} = 521 nm) and iodide (λ_{max} = 527 nm) clusters. In the copper bromide clusters, the emissions of **2** (λ_{max} = 521 nm) and **2**·$2CHCl_3$ (λ_{max} = 519 nm) are similar while simply changing the solvate to dichloromethane red-shifts the emission of **2**·$2CH_2Cl_2$ to 542 nm (Figure 6). A much more dramatic difference in emission maxima is observed in the copper iodide clusters. The emission of **3**·$0.5CH_2Cl_2$ (λ_{max} = 576 nm) is significantly red-shifted compared to that of the parent compound **3** (λ_{max} = 527 nm, Figure 7).

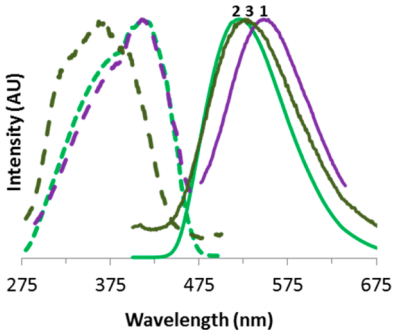

Figure 5. Normalized solid-state excitation (dashed lines) and emission (solid lines) spectra of **1**−**3**.

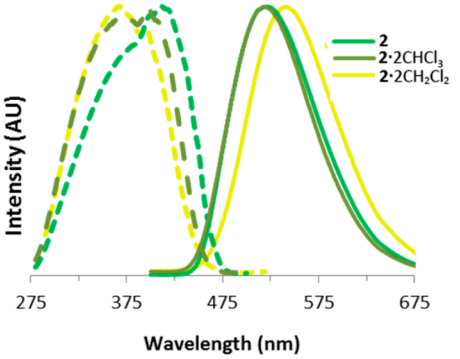

Figure 6. Normalized solid-state excitation (dashed lines) and emission (solid lines) spectra of **2**, **2**·$2CHCl_3$, and **2**·$2CH_2Cl_2$.

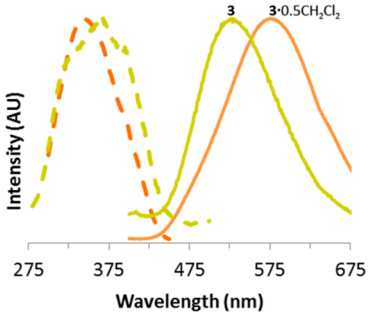

Figure 7. Normalized solid-state excitation (dashed lines) and emission (solid lines) spectra of **3** and **3**·$0.5CH_2Cl_2$.

Scheme 3. Crystallization of Different Forms of $Cu_4Br_4(PPh_2py)_2$

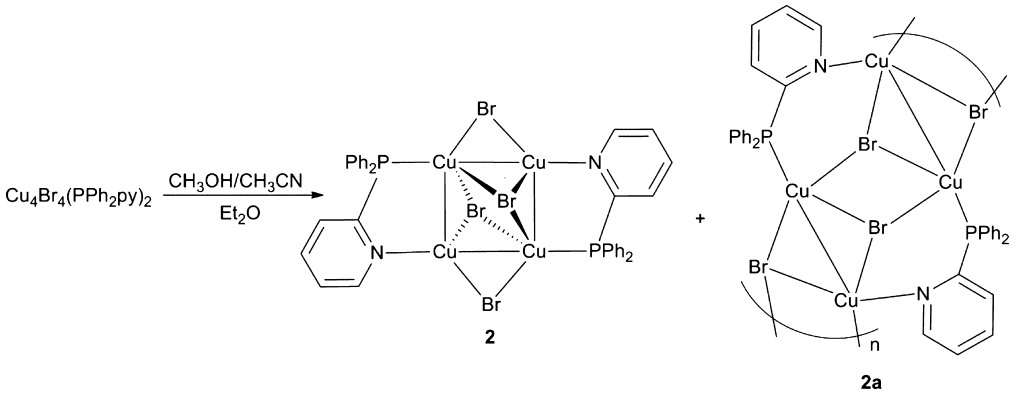

DOI: 10.1021/acs.inorgchem.5b00443
Inorg. Chem. 2015, 54, 6245−6256

Electronic structure calculations were performed to gain insight into the nature of the electronic transitions observed in the $Cu_4X_4L_2$ clusters. With a focus on X = Br, initial single point calculations were performed at the MP2/def2-tzvp level on the singlet electronic configurations for **2**, **2**·$2CH_2Cl_2$, and **2**·$2CHCl_3$ utilizing the crystallographic coordinates obtained for the three complexes. These calculations were performed only on the isolated Cu_4Br_4 molecules (in the absence of solvent) to determine the influence of the distortion of the Cu_4Br_4 core on the frontier molecular orbitals. The HOMOs for the series, which are primarily Br(4p)/Cu(3d) σ-antibonding in nature, displayed a destabilization going from **2**·$2CHCl_3$ to **2** to **2**·$2CH_2Cl_2$ (Figure 8). The LUMOs for the three complexes,

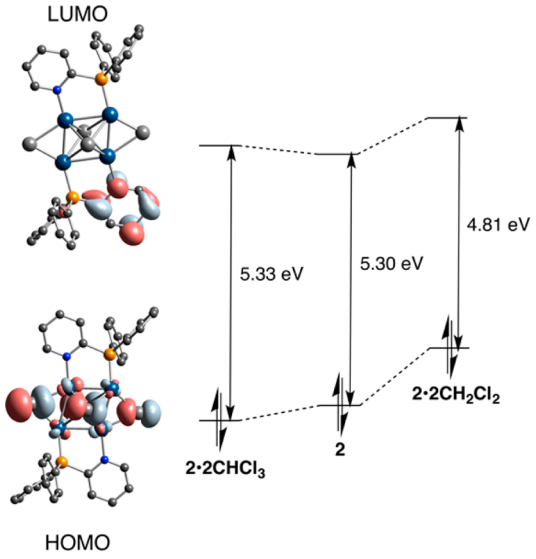

Figure 8. Isosurface plots of the HOMO and LUMO of Cu_4Br_4 molecules at the **2**·$2CHCl_3$ geometry, which are virtually identical to the HOMO and LUMO of **2** and **2**·$2CH_2Cl_2$. The HOMO and LUMO energies from the MP2 calculations are plotted relative to the energy of the HOMO for **2**·$2CHCl_3$.

which are primarily pyridyl π^* in character, do not follow the trends obtained for the HOMO with the LUMO calculated for **2**·$2CH_2Cl_2$ being the most destabilized, followed by **2**·$2CHCl_3$ and finally **2**. This demonstrates that subtle changes in the geometry of the complexes have a large influence on the resulting MO energy levels. Oddly, the trend observed in the energies of the HOMO/LUMO gaps obtained for the three complexes follow the experimentally observed trends of the emission, not excitation, energies (**2**·$2CHCl_3$ > **2** > **2**·$2CH_2Cl_2$). We note that similar results were obtained at the PBE0/def2-tzvp level of theory with dispersion correction suggesting that such a level of theory is capable of treating these systems.

The excitation and emission energies were obtained within the time dependent density functional theory (TD-DFT) formalism. Prior to performing these calculations, geometry optimizations (**GO**) of the isolated Cu_4Br_4 molecule for the singlet and triplet spin states were performed at the PBE0/def2-tzvp level with a dispersion correction producing ^{1}**2·GO** and ^{3}**2·GO**. XYZ coordinates of ^{1}**2·GO** and ^{3}**2·GO** are presented in Tables S25 and S26 in the Supporting Information. The singlet state geometry compares well with the crystallographic structure of **2** (Figure 9a). Surprisingly, optimization of the triplet state yielded only a slight distortion of the molecule in

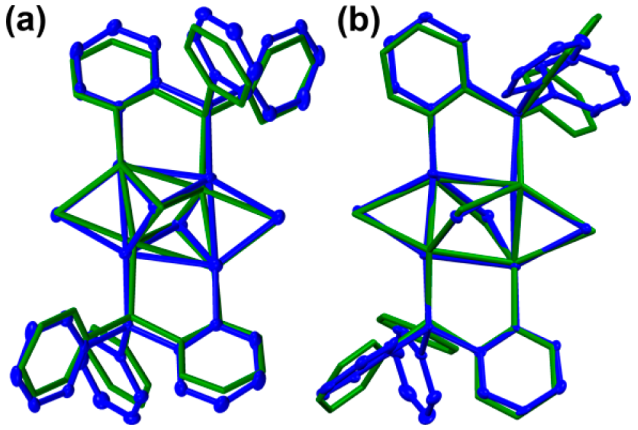

Figure 9. Overlay of the computationally derived structure of ^{1}**X·GO** (green) and X-ray crystal structure of **X** (blue) for (a) X = **2** and (b) X = **3**.

comparison to the singlet state geometry. The resulting $S_{1/2} \leftarrow S_0$ excitations can be best described as a Cu_4Br_4 core to pyridyl ligand charge transfer transition (Figures S26 and S27 and Tables S27−S30 in the Supporting Information). The resulting excitation energy for the two lowest energy transitions, which correspond to quasidegenerate excited states, agree well with the observed lowest energy excitation transition (422.6/422.3 nm). The next highest energy transitions, which are also Cu_4Br_4 core to pyridyl transitions, are ~2400 cm^{-1} higher in energy and have oscillator strengths over an order of magnitude lower than the $S_{1/2} \leftarrow S_0$ excitations. The resulting $T_1 \rightarrow S_0$ emission is primarily a pyridyl ligand to Cu_4Br_4 core charge transfer transition and occurs at an energy of 531.6 nm, which also corresponds well with the emission energy obtained for **2** (and **2**·$2CHCl_3$).

In an analogous manner, the excitation and emission energies of **3** were also probed. Geometry optimizations (PBE0/def2-tzvp/D3) on the singlet and triplet surfaces yielded ^{1}**3·GO** and ^{3}**3·GO**, respectively. As observed with **2·GO**, there was little deviation in the structure of **3·GO** upon promoting **3·GO** from the singlet and triplet surface. The resulting structure of ^{1}**3·GO** compares well with the crystal structure of **3** (Figure 9b). Similar to **2·GO**, the lowest energy transitions that correspond to $S_n \leftarrow S_0$ excitations (n = 1−3) for **3·GO** are Cu_4I_4 core to pyridyl ligand charge transfer transitions. These transitions are comparatively closer in energy than those obtained for **2·GO** (1500 cm^{-1}) and have similar oscillator strengths. As observed with **2·GO**, the resulting $T_1 \rightarrow S_0$ emission obtained for **3·GO** is best described as a pyridyl ligand to Cu_4I_4 core charge transfer transition and occurs at an energy similar to that obtained for **3**·$0.5CH_2Cl_2$ (572.3 vs 576 nm^2).

DISCUSSION

Despite the rigidity of the PPh_2py ligand, the Cu_4X_4 cores of clusters **1**−**3** and their solvates are remarkably flexible, and this has a significant consequence on the optical properties. There are few examples of octahedral $Cu_4X_4L_2$ clusters with phosphine ligands reported.[23,28,29,40−44] In 2004, Che and co-workers reported the octahedral Cu_4I_4(dcpm)$_2$ complex where dcpm = bis(dicyclohexylphosphino)methane.[23] Similar to clusters **1**, **2**, **2**·$2CH_2Cl_2$, and **2**·$2CHCl_3$, the Cu_4I_4(dcpm)$_2$ structure features two halides which doubly bridge adjacent copper centers. However, the remaining two iodide ions bridge all four copper centers approximately equally. This μ_4 bonding

DOI: 10.1021/acs.inorgchem.5b00443
Inorg. Chem. 2015, 54, 6245−6256

motif is seen in several other reported octahedral complexes.[23,29,40−42,44] At 77 K, $Cu_4I_4(dcpm)_2$ exhibits dual emission with high and low energy emission bands. Analogous to previous studies on copper cubanes, Che and co-workers suggested that the nature of the high energy emission was based on a copper-centered 3d → 4s,4p excited state perturbed by cuprophilic interactions in the cluster.[23] Interestingly, the analogous copper iodide cluster with dppm (bis-(diphenylphosphino)methane) has triply bridging iodide ions instead of the quadruply bridging iodide ions found in $Cu_4I_4(dcpm)_2$.[28] The μ_3-halide bonding motif is found in many octahedral complexes[28,29,43,44] including the copper chloride and bromide clusters, **1**, **2**, **2**·$2CH_2Cl_2$, and **2**·$2CHCl_3$ presented here. The core geometry is also influenced by the bridging halide. Though the related clusters $Cu_4I_4(dppm)_2$ and $Cu_4Cl_4(dppm)_2$ both have μ_3-halide bonding, the Cu−Cu distances in the two clusters vary dramatically. In $Cu_4Cl_4(dppm)_2$, the Cu−Cu distances are similar to Cu1−Cu2 = 2.958(4) Å and Cu1−Cu2A = 2.992(3) Å. However, in $Cu_4I_4(dppm)_2$, the cluster has a nonbonding Cu1···Cu2 interaction of 3.1086(11) Å and a shorter Cu1−Cu2A bond of 2.6836(10) Å.[28] This difference in Cu−Cu bond lengths is also observed in copper iodide clusters **3** and **3**·$0.5CH_2Cl_2$ though the longest and shortest bond lengths only differ by 0.2 Å.

Of the reported octahedral copper clusters, there are a variety of structural motifs dependent on phosphine ligand and bridging halide. The Cu−Cu distances of the reported clusters range widely from 2.747(2) to 3.0348(14) Å, and the intermetallic angles range from 75.15(9)° to 104.85(9)°.[23,28,29,40−44] The clusters **1**, **2**, **2**·$2CH_2Cl_2$, **2**·$2CHCl_3$, **3**, and **3**·$0.5CH_2Cl_2$ all have Cu−Cu distances within the lower end of the reported range, and copper iodide clusters **3** and **3**·$0.5CH_2Cl_2$ have Cu−Cu distances (2.5 Å) lower than the reported range. Though the reported clusters have a large range of intermetallic angles, the halide bonding of the clusters possibly influences the core geometry. Clusters with μ_4-halide bonding have rectangular copper cores with intermetallic angles ranging from 83.49(2)° to 96.51(2)°, and those with μ_3-halide bonding have cores resembling a parallelogram with intermetallic angles ranging from 75.15(9)° to 81.51(5)° for acute angles and 98.49(5)° to 104.85(9)° for the others. Though it is difficult to generalize on the basis of the limited number of octahedral clusters, it is possible that the clusters with cores resembling a parallelogram have μ_3-halide bonding because the halide ions are closer to the copper centers forming the acute intermetallic angles of the core. This proposed trend, however, is not seen in the copper chloride and bromide clusters reported here. Though all copper chloride and bromide clusters have μ_3-halide bonding, clusters **1** and **2**·$2CH_2Cl_2$ have rectangular cores and clusters **2** and **2**·$2CHCl_3$ have skewed cores. In these copper halide clusters, it is difficult to determine the influences of the core geometry and halide bonding on each other.

Interestingly, all of the previously reported $Cu_4X_4L_2$ clusters have planar Cu_4-cores regardless of the halide or bridging ligand. The distorted butterfly structural motif of **3** and **3**·$0.5CH_2Cl_2$ does not resemble any of the previously reported $Cu_4X_4L_2$ clusters. While it is possible that the rigidity of the PPh_2py ligand is responsible for this new structural motif, it cannot be the sole cause because the analogous chloride and bromide clusters have planar cores. Additionally, Mathey and co-workers also observed a planar Cu_4-core in the $Cu_4I_4L_2$ cluster with the closely related and equally rigid phosphinine ligand, 2,4-diphenyl-5-methyl-6-(2,3-dimethylphenyl)-phosphinine.[40]

Of the reported octahedral clusters, only a few clusters have been characterized photophysically.[23,43] Thompson and co-workers reported several $Cu_4I_4(L)_2$ clusters supported by a bridging 2-[(diorganophosphino)methyl]pyridine ligand that, depending on the substituents on the phosphine, exhibit single or dual emission. The dual emission of the clusters is reminiscent of that of copper cubanes. DFT calculations on these clusters suggest that the high energy emission band originates from a (M + X)LCT process while the low energy emission band was assigned to a ^{3}CC process.[44]

Remarkably, the subtle structural differences in **1**−**3** and their solvates produce significant differences in the emission. Unlike copper cubane clusters, the clusters **1**−**3** all have single temperature-independent emission as shown in Figures S21−S23 in the Supporting Information. The presence of only low energy emission bands suggests the absence of the high energy ^{3}CC transitions found in other copper halide clusters. Though the Cu−Cu distances are all less than 2.8 Å, it is possible that the rigidity of the PPh_2py ligand prevents the copper core distortion required for ^{3}CC transitions. As determined by MP2 and DFT calculations on the copper bromide and iodide clusters, the HOMOs of the copper clusters are both copper and halide centered, and the LUMOs are predominately pyridyl π^* in nature. TD-DFT calculations suggest that the low energy excitations and the resulting $T_1 \rightarrow S_0$ emissions are Cu_4X_4 to pyridyl π^* in nature; we find no evidence of copper core-centered transitions by TD-DFT methods. The assignment of the emission for **1**−**3** as a (M + X)LCT emission is therefore consistent with the emissions observed in related dinuclear $Cu_2X_2L_3$ compounds extensively studied by Baumann, Bräse, and co-workers.[4,21,32,47,48] We note that excited state geometry optimizations of both **2** and **3** indicate minimal distortion of the complex upon promotion to the triplet surface. This seems to indicate that the changes in the emissive properties of the complexes are largely electronic in nature. It is also possible that the differences in crystal packing of the solvated versus unsolvated forms allow for larger excited state distortions. If this is the case, it is possible that the computational methods (PBE0/D3, which gave nearly identical results as MP2 level calculations) used do not fully capture the underlying physics of the systems investigated.

Although qualitatively similar to one another in terms of the degree of excited state distortions and the nature of the $S_1 \leftarrow S_0$ excitation and $T_1 \rightarrow S_0$ emissions, the TD-DFT calculations do show differences between the two in terms of the energy and nature of the transitions. Focusing on the $S_1 \leftarrow S_0$ excitation, the energy of the lowest energy excitation for **2·GO** versus **3·GO** is blue-shifted by over 2500 cm^{-1}. Furthermore, the oscillator strengths of the two lowest energy singlet excitations obtained for **3·GO** are over an order of magnitude smaller than those observed in the Cu_4Br_4 system. We attribute this to fundamental differences in the copper halide bonding of the two complexes; the calculations suggest an overall reduction in copper halide covalency for **3·GO** versus **2·GO.** The lowered covalency of the Cu−I versus Cu−Br bond creates largely I-dominated donor-states with little Cu-pyridyl character for **3·GO**, while **2·GO** contains a significantly larger degree of Cu-pyridyl character in the lowest energy donor states.

Due to the unique butterfly cores of **3** and **3**·$0.5CH_2Cl_2$, it is difficult to compare the emission of the copper iodide clusters

DOI: 10.1021/acs.inorgchem.5b00443
Inorg. Chem. 2015, 54, 6245−6256

to those of the octahedral copper chloride and bromide clusters. However, the nearly superimposable (Figure S15 in Supporting Information) copper chloride **1** and copper bromide **2** clusters can be compared. The excitation profiles of **1** and **2** are remarkably similar though the emission of **1** is red-shifted compared to that of **2**. Similar observations were reported by Sasaki and co-workers in the iodide and bromide analogs of $Cu_2X_2(\mu$-1,8-naphthyridine$)(PPh_3)_2$.[19] To probe the role of the halide, Ford, Palke, and co-workers performed *ab initio* studies on various structurally similar $Cu_4X_4L_4$ clusters with XLCT emission.[49] In the isostructural $Cu_4X_4(dpmp)_4$ compounds where dpmp = 2-(diphenylmethyl)pyridine, the emission energies are highest when X = I and lowest for X = Cl though the excitation spectra were unchanged.

An interesting comparison can be made for the copper iodide cluster **3** and its solvate **3**·0.5CH_2Cl_2 which have nearly superimposable cluster geometries (Figure S18 in Supporting Information), but the emission of **3**·0.5CH_2Cl_2 (576 nm) is red-shifted compared to that of **3** (527 nm). Beyond the cluster, both crystalline solids contain nearly identical $\pi_{Py}-\pi_{Ph}$ interactions of 3.6 Å. The only significant structural difference is an additional solvate Cl$-\pi_{Py}$ interaction (3.8 Å) in **3**·0.5CH_2Cl_2. The incorporation of the Cl$-\pi_{py}$ interaction appears to stabilize the pyridyl π^* orbital and hence red-shift the emission.

In contrast to the copper iodide clusters, the copper bromide clusters all feature different core geometries and halide bonding making it difficult to separate the various influences of core geometry, halide, and cluster−solvent interactions on the emission. Like the iodo analogues a similar red-shift in emission was observed for **2** (λ_{max} = 521 nm) and **2**·2CH_2Cl_2 (λ_{max} = 542 nm). Replacing the dichloromethane with chloroform produces a crystal (**2**·2$CHCl_3$) with similar Cl$-\pi_{py}$ interactions; however, this material emits slightly higher in energy relative to that of **2**. As shown in Figure S10 in the Supporting Information, there are many intermolecular $\pi-\pi$ and Cl$-\pi$ interactions within the extended lattice of **2**·2$CHCl_3$. Additionally, as presented in Tables 3−5, there are considerable differences in the core structures of **2**, **2**·2CH_2Cl_2, and **2**·2$CHCl_3$ which would influence the energy of the HOMOs, further complicating the analysis.

Copper halide clusters have been extensively studied due to their potential application in OLEDs.[6,33−36] Recently, Volz et al.[32] reported that the solution processing of Cu(I) phosphine complexes in optoelectronic device fabrication often produces materials with inconsistent emissive proprieties. Originally thought to originate from complex decomposition or dissociation, measurements on single crystals, thin films, and powders suggest the emitting complexes remain intact in these materials. Volz et al. suggest that "a combination of rigidochromic effects with a distortion of the ground-state geometry of the complexes" accounts for the observed differences in excited state properties. The work presented here supports their conclusions. The observation of marked differences in emission maxima through simple crystallization of clusters **1**−**3** from common solvent underscores the importance of recognizing solvate−complex and other noncovalent interactions on material processing. The observation of different core geometries as a function of halide and solvate was surprising and illustrates the high plasticity of the $Cu_4X_4L_2$ cluster cores. These subtle differences in metal−metal and metal−ligand bonding, which additionally affect the (M + X)LCT excited states, greatly complicate the rational design of copper halide clusters as luminescent materials. However, through judicious choice of solvent, ligand, and halide one might be able to develop a series of material with desirable properties.

CONCLUSION

Co-crystallization of the octahedral and butterfly shaped $Cu_4X_4L_2$ from various solvents produces clusters and their solvates with a remarkable variety of structural motifs. These motifs feature differences in the copper cores and μ-halide bonding which subtly perturb the emission of the copper halide clusters. Unlike copper cubane clusters, these $Cu_4X_4L_2$ clusters exhibit a single temperature-independent emission band that, based on TD-DFT calculations, is assigned to a mixed metal- and halide-to-ligand charge transfer (M + X)LCT consistent with that of analogous copper dimers. The significant structural rearrangements observed in the Cu_4X_4 core and subsequent changes in optical properties induced by simple solvent inclusion in the crystal lattice have important implications for the consistent processing of copper phosphine clusters as materials for optoelectronic applications.

EXPERIMENTAL SECTION

All chemicals were used as received. NMR spectra were recorded at 25 °C on Varian 400-MR and V500 spectrometers at the indicated frequencies. The ^{1}H NMR spectra were referenced to the residual solvent signal (CH_3CN at 1.94 ppm), and the $^{31}P\{^1H\}$ NMR spectrum was referenced to 85% H_3PO_4. Solution UV−vis spectra were obtained using a Hewlett-Packard 8453 diode array spectrometer (1 cm path-length quartz cells), and solid-state UV−vis spectra were obtained using a Varian Cary 300 Bio UV−vis spectrophotometer equipped with a Labsphere DRA-CA-3300 integrating sphere. Excitation and emission spectra were recorded on a Jobin Yvon Horiba FluoroMax-3 instrument. All samples were excited at 365 nm unless otherwise stated.

Synthesis of Clusters. The synthesis of $Cu_4Cl_4(PPh_2py)_2$ (**1**) follows: A round bottomed flask was charged with CuCl (108 mg, 1.09 mmol) and PPh_2py (145 mg, 0.551 mmol) followed by 100 mL of 1:1 mixture of dichloromethane/acetonitrile. The resulting yellow solution was stirred for 20 min and then concentrated under vacuum. The solution was precipitated with diethyl ether to form **1** as a tan solid. Yield: 46 mg (19%). Crystals were obtained by vapor diffusion of diethyl ether into a dichloromethane or acetonitrile solution to form **1** or **1a**, respectively. ^{1}H NMR (500 MHz, CD_3CN): δ 9.22 (br, 2H), 7.92 (br, 2H), 7.39−7.73 (br, 11H), 7.30−7.33 (br, 6H), 7.19−20 (br, 7H). $^{31}P\{^1H\}$ NMR (161 MHz, CD_3CN): δ 4.92 (br). UV (CH_2Cl_2) λ_{max} nm (ε): 256 (30 000).

The synthesis of $Cu_4Br_4(PPh_2py)_2$ (**2**) follows: This material was prepared analogously to **1** using CuBr (162 mg, 0.564 mmol) and PPh_2py (154 mg, 0.584 mmol) to produce a tan solid. Yield: 258 mg (83%). Crystals were obtained by vapor diffusion of diethyl ether into solutions of methanol/acetonitrile, chloroform, and dichloromethane to form **2**, **2**·2$CHCl_3$, and **2**·2CH_2Cl_2, respectively. Crystals of **2a** were also obtained from the methanol/acetonitrile solution. ^{1}H NMR (400 MHz, CD_3CN): δ 8.95 (br, 2H), 7.84−7.86 (br, 2H), 7.30−7.54 (br, 24H). UV (CH_2Cl_2) λ_{max} nm (ε): 250 (35 000).

The synthesis of $Cu_4I_4(PPh_2py)_2$ (**3**) follows: The material was prepared analogously to **1** using CuI (198 mg, 1.04 mmol) and PPh_2py (137 mg, 0.521 mmol) to produce a yellow solid. Yield: 212 mg (63%). Crystals were obtained by vapor diffusion of diethyl ether into solutions of acetonitrile and dichloromethane to form **3** and **3**·0.5CH_2Cl_2, respectively. ^{1}H NMR (400 MHz, CD_3CN): δ 8.86 (br), 7.82 (br), 7.45 (br), 7.37 (br). UV (CH_2Cl_2) λ_{max} nm (ε): 250 (12 000).

X-ray Crystallography. Single crystal X-ray diffraction was performed on a Bruker SMART Apex CCD instrument at 100 K using graphite-monchromated Mo Kα radiation. The crystals were

DOI: 10.1021/acs.inorgchem.5b00443
Inorg. Chem. 2015, 54, 6245−6256

covered in Paratone oil and mounted on glass fibers. Lorentz and polarization effects were corrected using SAINT, and the absorption corrections were applied using SADABS and TWINABS (**2**·2$CHCl_3$).[50,51] The structures were solved using direct methods or Patterson syntheses using OLEX2.[52] Due to poor quality data of **3**·0.5CH_2Cl_2, the carbon atoms were only refined isotropically. The figures of individual crystal structures were prepared using Diamond 3, and the overlays were prepared using Mercury 3.1.[53,54]

Computational Methods. Electronic structure calculations were performed using *ORCA* 2.9 and 3.0.[55] Geometry optimizations and single point energies were performed using the PBE0 hybrid density functional[56] with the def2-tzvp basis set on all atoms[57,58] and atomic pairwise dispersion correction with Becke–Johnson damping.[59] Excitation and emission energies for the geometry optimized structures of **2** and **3** were determined by employing the TD-DFT formalism. Single point energies for the core structures of **2**, **2**·2CH_2Cl_2, and **2**·2$CHCl_3$ were calculated at the MP2 level using the def2-tzvp basis set on all atoms. Atomic populations to the MOs were calculated using a Löwdin population analysis.[60] Isosurface plots were generated using the program *LUMO* 1.0.1.[61]

■ ASSOCIATED CONTENT

Supporting Information

X-ray crystallographic data for the complexes in CIF format; overlay plots; characterization of the compounds, including NMR and optical spectra; complete X-ray structural characterization, including thermal ellipsoid plots, and tables of bond distances and angles; and computational details. The Supporting Information is available free of charge on the ACS Publications website at DOI: 10.1021/acs.inorgchem.5b00443.

■ AUTHOR INFORMATION

Corresponding Author

*E-mail: vjc@unr.edu.

Notes

The authors declare no competing financial interest.

■ ACKNOWLEDGMENTS

This material is based upon work supported by the National Science Foundation under Grant CHE-1362662 (J.S.).

■ REFERENCES

(1) Kyle, K. R.; Ryu, C. K.; Ford, P. C.; DiBenedetto, J. A. *J. Am. Chem. Soc.* **1991**, *113*, 2954–2965.
(2) Ford, P. C.; Vogler, A. *Acc. Chem. Res.* **1993**, *26*, 220–226.
(3) Ford, P. C.; Cariati, E.; Bourassa, J. *Chem. Rev.* **1999**, *99*, 3625–3648.
(4) Wallesch, M.; Volz, D.; Zink, D. M.; Schepers, U.; Nieger, M.; Baumann, T.; Bräse, S. *Chem.—Eur. J.* **2014**, *20*, 6578–6590.
(5) Benito, Q.; Le Goff, X. F.; Maron, S.; Fargues, A.; Garcia, A.; Martineau, C.; Taulelle, F.; Kahlal, S.; Gacoin, T.; Boilot, J.-P.; Perruchas, S. *J. Am. Chem. Soc.* **2014**, *136*, 11311–11320.
(6) Zou, L.-Y.; Cheng, Y.-X.; Li, Y.; Li, H.; Zhang, H.-X.; Ren, A.-M. *Dalton Trans.* **2014**, *43*, 11252–11259.
(7) Perruchas, S.; Tard, C.; Le Goff, X. F.; Fargues, A.; Garcia, A.; Kahlal, S.; Saillard, J.-Y.; Gacoin, T.; Boilot, J.-P. *Inorg. Chem.* **2011**, *50*, 10682–10692.
(8) Lapprand, A.; Dutartre, M.; Khiri, N.; Levert, E.; Fortin, D.; Rousselin, Y.; Soldera, A.; Jugé, S.; Harvey, P. D. *Inorg. Chem.* **2013**, *52*, 7958–7967.
(9) Kitagawa, H.; Ozawa, Y.; Toriumi, K. *Chem. Commun.* **2010**, *46*, 6302–6304.
(10) Tran, D.; Bourassa, J. L.; Ford, P. C. *Inorg. Chem.* **1997**, *36*, 439–442.
(11) Shan, X.-C.; Jiang, F.-L.; Chen, L.; Wu, M.-Y.; Pan, J.; Wan, X.-Y.; Hong, M.-C. *J. Mater. Chem. C* **2013**, *1*, 4339–4349.
(12) Li, Y.; Yung, K.-F.; Chan, H.-S.; Wong, W.-T. *Inorg. Chem. Commun.* **2003**, *6*, 1451–1453.
(13) Kumar, S.; Mani, G.; Dutta, D.; Mishra, S. *Inorg. Chem.* **2014**, *53*, 700–709.
(14) Roesch, P.; Nitsch, J.; Lutz, M.; Wiecko, J.; Steffen, A.; Müller, C. *Inorg. Chem.* **2014**, *53*, 9855–9859.
(15) Yuan, S.; Wang, H.; Wang, D.-X.; Lu, H.-F.; Feng, S.-Y.; Sun, D. *CrystEngComm* **2013**, *15*, 7792–7802.
(16) Di Nicola, C.; Koutsantonis, G. A.; Pettinari, C.; Skelton, B. W.; Somers, N.; White, A. H. *Inorg. Chim. Acta* **2006**, *359*, 2159–2169.
(17) Samanamú, C. R.; Lococo, P. M.; Woodul, W. D.; Richards, A. F. *Polyhedron* **2008**, *27*, 1463–1470.
(18) Tsuboyama, A.; Kuge, K.; Furugori, M.; Okada, S.; Hoshino, M.; Ueno, K. *Inorg. Chem.* **2007**, *46*, 1992–2001.
(19) Araki, H.; Tsuge, K.; Sasaki, Y.; Ishizaka, S.; Kitamura, N. *Inorg. Chem.* **2007**, *46*, 10032–10034.
(20) Sun, D.; Yuan, S.; Wang, H.; Lu, H.-F.; Feng, S.-Y.; Sun, D.-F. *Chem. Commun.* **2013**, *49*, 6152–6154.
(21) Volz, D.; Zink, D. M.; Bocksrocker, T.; Friedrichs, J.; Nieger, M.; Baumann, T.; Bräse, S.; Lemmer, U. *Chem. Mater.* **2013**, *25*, 3414–3426.
(22) Perruchas, S.; Le Goff, X. F.; Maron, S.; Maurin, I.; Guillen, F.; Garcia, A.; Gacoin, T.; Boilot, J.-P. *J. Am. Chem. Soc.* **2010**, *132*, 10967–10969.
(23) Fu, W.-F.; Gan, X.; Che, C.-M.; Cao, Q.-Y.; Zhou, Z.-Y.; Zhu, N. N.-Y. *Chem.—Eur. J.* **2004**, *10*, 2228–2236.
(24) Nixon, T. D.; Gamble, A. J.; Thatcher, R. J.; Whitwood, A. C.; Lynam, J. M. *Inorg. Chim. Acta* **2012**, *380*, 252–260.
(25) Schwerdtfeger, P.; Krawczyk, R. P.; Hammerl, A.; Brown, R. *Inorg. Chem.* **2004**, *43*, 6707–6716.
(26) Daly, S.; Haddow, M. F.; Orpen, A. G.; Rolls, G. T. A.; Wass, D. F.; Wingad, R. L. *Organometallics* **2008**, *27*, 3196–3202.
(27) Ahuja, R.; Nethaji, M.; Samuelson, A. G. *J. Organomet. Chem.* **2009**, *694*, 1144–1152.
(28) Nardin, G.; Randaccio, L. *Acta Crystallogr.* **1974**, *B30*, 1377–1379.
(29) Chandrasekhar, V.; Ahuja, R.; Nethaji, M.; Samuelson, A. G. *Inorg. Chim. Acta* **2011**, *372*, 220–226.
(30) Zink, D. M.; Baumann, T.; Friedrichs, J.; Nieger, M.; Bräse, S. *Inorg. Chem.* **2013**, *52*, 13509–13520.
(31) Monkowius, U.; Zabel, M.; Fleck, M.; Yersin, H. *Z. Naturforsch.* **2009**, *64b*, 1513–1524.
(32) Volz, D.; Wallesch, M.; Grage, S. L.; Göttlicher, J.; Steininger, R.; Batchelor, D.; Vitova, T.; Ulrich, A. S.; Heske, C.; Weinhardt, L.; Baumann, T.; Bräse, S. *Inorg. Chem.* **2014**, *53*, 7837–7847.
(33) Leitl, M. J.; Krylova, V. A.; Djurovich, P. I.; Thompson, M. E.; Yersin, H. *J. Am. Chem. Soc.* **2014**, *136*, 16032–16038.
(34) Leitl, M. J.; Küchle, F.-R.; Mayer, H. A.; Wesemann, L.; Yersin, H. *J. Phys. Chem. A* **2013**, *117*, 11823–11836.
(35) Lotito, K. J.; Peters, J. C. *Chem. Commun.* **2010**, *46*, 3690–3692.
(36) Keller, S.; Constable, E. C.; Housecroft, C. E.; Neuburger, M.; Prescimone, A.; Longo, G.; Pertegás, A.; Sessolo, M.; Bolink, H. J. *Dalton Trans.* **2014**, *43*, 16593–16596.
(37) Shan, X.-C.; Jiang, F.-L.; Yuan, D.-Q.; Wu, M.-Y.; Zhang, S.-Q.; Hong, M.-C. *Dalton Trans.* **2012**, *41*, 9411–9416.
(38) Vega, A.; Saillard, J.-Y. *Inorg. Chem.* **2004**, *43*, 4012–4018.
(39) Benito, Q.; Goff, X. F.; Le Nocton, G.; Fargues, A.; Garcia, A.; Berhault, A.; Kahlal, S.; Saillard, J.-Y.; Martineau, C.; Trébosc, J.; Gacoin, T.; Boilot, J.-P.; Perruchas, S. *Inorg. Chem.* **2015**, *54*, 4483–4494.
(40) Mézailles, N.; Le Floch, P.; Waschbüsch, K.; Ricard, L.; Mathey, F.; Kubiak, C. P. *J. Organomet. Chem.* **1997**, *541*, 277–283.
(41) Scherer, M.; Stein, D.; Breher, F.; Geier, J.; Schönberg, H.; Grützmacher, H. *Z. Anorg. Allg. Chem.* **2005**, *631*, 2770–2774.
(42) Kühnel, E.; Shishkov, I. V.; Rominger, F.; Oeser, T.; Hofmann, P. *Organometallics* **2012**, *31*, 8000–8011.

DOI: 10.1021/acs.inorgchem.5b00443
Inorg. Chem. 2015, 54, 6245–6256

(43) Camus, A.; Nardin, G.; Randaccio, L. *Inorg. Chim. Acta* **1975**, *12*, 23−32.
(44) Liu, Z.; Djurovich, P. I.; Whited, M. T.; Thompson, M. E. *Inorg. Chem.* **2012**, *51*, 230−236.
(45) Chen, K.; Strasser, C. E.; Schmitt, J. C.; Shearer, J.; Catalano, V. J. *Inorg. Chem.* **2012**, *51*, 1207−1209.
(46) Hofbeck, T.; Monkowius, U.; Yersin, H. *J. Am. Chem. Soc.* **2015**, *137*, 399−404.
(47) Bergmann, L.; Friedrichs, J.; Mydlak, M.; Baumann, T.; Nieger, M.; Bräse, S. *Chem. Commun.* **2013**, *49*, 6501−6503.
(48) Zink, D. M.; Bächle, M.; Baumann, T.; Nieger, M.; Kühn, M.; Wang, C.; Klopper, W.; Monkowius, U.; Hofbeck, T.; Yersin, H.; Bräse, S. *Inorg. Chem.* **2013**, *52*, 2292−2305.
(49) Vitale, M.; Ryu, C. K.; Palke, W. E.; Ford, P. C. *Inorg. Chem.* **1994**, *33*, 561−566.
(50) *SAINT: Program for Data Reduction, Version 7.68A*; Bruker AXS: Madison, WI, 2009.
(51) Sheldrick, G. M. *Acta Crystallogr., Sect. A: Found. Crystallogr.* **2008**, *64*, 112−122.
(52) Dolomanov, O. V.; Bourhis, L. J.; Gildea, R. J.; Howard, J. A. K.; Puschmann, H. *J. Appl. Crystallogr.* **2009**, *42*, 339−341.
(53) Brandenburg, K.; Putz, H. *Diamond-Crystal and Molecular Structure Visualization*; Crystal Impact: Bonn, Germany, 2009.
(54) Macrae, C. F.; Bruno, I. J.; Chisholm, J. A.; Edgington, P. R.; McCabe, P.; Pidcock, E.; Rodriguez-Monge, L.; Taylor, R.; van de Streek, J.; Wood, P. A. *J. Appl. Crystallogr.* **2008**, *41*, 466−470.
(55) Nesse, F. *Wiley Interdiscip. Rev.: Comput. Mol. Sci.* **2012**, *2*, 73−78.
(56) Adamo, C.; Barone, V. J. *Chem. Phys.* **1999**, *110*, 6158−6169.
(57) Weigend, F.; Ahlrichs, R. *Phys. Chem. Chem. Phys.* **2005**, *7*, 3297−3305.
(58) Weigend, F.; Ahlrichs, R. *Phys. Chem. Chem. Phys.* **2006**, *8*, 1057−1065.
(59) Grimme, S.; Ehrlich, S.; Goerigk, L. *J. Comput. Chem.* **2011**, *32*, 1456−1465.
(60) Szabo, A.; Ostlund, N. S. *Modern Quantum Chemistry: Introduction to Advanced Electronic Structure Theory*; Dover Publications: Mineola, NY, 1989.
(61) Kieber-Emmons, M. T. *Lumo, Version 1.0.1*; Ephrata, PA, 2012.

DOI: 10.1021/acs.inorgchem.5b00443
Inorg. Chem. 2015, 54, 6245−6256